



UNIVERSITY OF LEEDS

This is a repository copy of *Event-driven fuzzy L^∞ control of DC microgrids under cyber attacks and quantization*.

White Rose Research Online URL for this paper:

<https://eprints.whiterose.ac.uk/214492/>

Version: Accepted Version

Article:

Li, F., Gao, L., Li, K. orcid.org/0000-0001-6657-0522 et al. (1 more author) (2024) Event-driven fuzzy L^∞ control of DC microgrids under cyber attacks and quantization.

Transactions of the Institute of Measurement and Control. ISSN 0142-3312

<https://doi.org/10.1177/01423312241265781>

© The Author(s) 2024. This is an author produced version of an article published in Transactions of the Institute of Measurement and Control. Uploaded in accordance with the publisher's self-archiving policy.

Reuse

Items deposited in White Rose Research Online are protected by copyright, with all rights reserved unless indicated otherwise. They may be downloaded and/or printed for private study, or other acts as permitted by national copyright laws. The publisher or other rights holders may allow further reproduction and re-use of the full text version. This is indicated by the licence information on the White Rose Research Online record for the item.

Takedown

If you consider content in White Rose Research Online to be in breach of UK law, please notify us by emailing eprints@whiterose.ac.uk including the URL of the record and the reason for the withdrawal request.



eprints@whiterose.ac.uk
<https://eprints.whiterose.ac.uk/>

Event-driven fuzzy \mathcal{L}_∞ control of DC microgrids under cyber attacks and quantization

Journal Title

XX(X):2–26

©The Author(s) 2024

Reprints and permission:

sagepub.co.uk/journalsPermissions.nav

DOI: 10.1177/ToBeAssigned

www.sagepub.com/

SAGE

Fuqiang Li^{1,*}, Lisai Gao¹, Kang Li², Chen Peng³

Abstract

This paper investigates the event-driven fuzzy \mathcal{L}_∞ control of direct-current (DC) microgrids subject to deception attacks, persistent bounded (PB) disturbances, premise mismatching, quantizer and delays. Firstly, using states of the fuzzy plant and a constant, a Zeno-free dynamic event-triggered mechanism (ETM) is presented, which is more robust to the PB disturbances than the static state-related ETMs (SSRETMs). Secondly, by virtually dividing the updating intervals of the controller, a unified time-delay fuzzy system model is established, which takes effects of dynamic ETM, deception attacks, disturbances, quantizer and delays into account. Thirdly, criteria for globally exponentially ultimately bounded (GEUB) stability in mean square with guaranteed \mathcal{L}_∞ -gain are obtained, and the quantitative relationship between the ultimate bound and the dynamic ETM is established. To overcome the inconvenience of the emulation method requiring two design steps, a co-design strategy is provided to simultaneously design the ETM and fuzzy controller subject to premise mismatching. Simulation results confirm that, even with the triggering rate 36.9% and the attacking rate 11.4%, satisfactory control performance can still be achieved; the dynamic ETM achieves better triggering performance than the SSRETMs; and the proposed controller achieves shorter settling time and smaller overshoot than the robust linear controller.

Keywords

DC microgrids, fuzzy control, false data injection attacks, event-triggered control, persistent bounded disturbances

Introduction

To reduce green-house gas emissions in addressing the climate change challenge, the microgrids provide viable solution to integrate the distributed renewable energy resources into power systems (Prasad, 2023). Due to the high penetration of DC power sources (e.g., solar photovoltaics and batteries) and DC loads (e.g., computers and light-emitting diodes), DC microgrids are attracting increasing attention in the last decade (Jiao et al., 2023). Besides, many problems in alternating-current (AC) microgrids such as reactive power flow, synchronization and harmonics do not exist in DC microgrids. Therefore, DC microgrids are being increasingly used in electric vehicles, renewable power plants, data centers, etc.

Using modern power electronics devices, loads in DC microgrids can consume constant power. The constant power loads (CPLs) has the feature of negative impedance, which often results in underdamping or unstable oscillation (Samanta et al., 2021). To this end, passive damping strategy (e.g., adding hardware such as capacitors and/or resistors), is proposed (Cespedes et al., 2011), which is effective and simple. However, due to physical constraints, it is often difficult and costly to implement this method. By changing the control loops to imitate passive elements such as virtual impedance or virtual resistor, active damping strategy is presented (Fan et al., 2022). However, by using small-signal models, this method only ensures small-signal stability (Xu et al., 2021). An alternative method, called T-S fuzzy strategy, can guarantee global stability and approximate nonlinear systems well (Hu et al., 2022), which makes it interesting to explore a fuzzy control method for DC microgrids with CPLs.

Nowadays, as communication networks are greatly integrated with the microgrids, they bring distinctive advantages, e.g., high scalability and flexibility, low cost of installation and maintenance. However, communication networks make microgrids vulnerable to cyber attacks, which mainly include false data injection (FDI) attacks and denial-of-service (DoS) attacks. DoS attacks prevent data transmission by blocking networks (Xing et al., 2023), while FDI attacks destroy data integrity and authenticity by injecting false data (Hossain et al., 2022). Since malicious adversaries can intentionally design the false injection signals to bypass general intrusion detection systems, the stealthy FDI attacks

¹ College of Sciences, Henan Agricultural University, Zhengzhou, China

² School of Electronic and Electrical Engineering, University of Leeds, Leeds, UK

³ Shanghai Key Laboratory of Power Station Automation Technology, School of Mechatronics Engineering and Automation, Shanghai University, Shanghai, China

Corresponding author:

Fuqiang Li, College of Sciences, Henan Agricultural University, No.63 Nongye Road, Zhengzhou 450052, China.
Email: lifuqiang@henau.edu.cn

are more destructive, and getting more attention. For instance, considering the FDI signals attacking the control signal, and using leader-following multi-agent system consensus method, the work (Xie and Wu, 2023) proposes a distributed fault-tolerant secondary control strategy for DC microgrids. Considering the constant-value FDI signals attacking the DC-bus voltage, the work (Habibi et al., 2022) designs a model predictive controller to detect and mitigate the attacks. Considering the FDI signals attacking the output current of distributed generation units, the work (Cecilia et al., 2022) designs an observer and proposes a control strategy for microgrids with CPLs. Considering the FDI signals attacking both of the current and voltage measurements, the work (Zhou et al., 2023) presents an integrated distributed control strategy.

To facilitate system analysis based on existing control theories, the aforementioned works adopt continuous control strategies. However, it is difficult to realize a continuous controller in practice. Besides, when system is running at the equilibrium point, it is often a waste of system resources to still execute control signals with a high frequency. To this end, the event-triggered control (ETC) strategy is designed (Peng and Li, 2018), which executes control laws only when system is running far away from the equilibrium point. Due to its distinctive advantage, the ETC strategy has been getting more attention in power systems. For instance, using the load current sharing error and regulation error of voltage observer to design the ETM, the work in (Peng et al., 2021) presents a distributed ETC strategy for DC microgrid. Removing the voltage observer in (Peng et al., 2021) by transforming both of voltage and current control into an optimization problem, the work (Shi et al., 2021) uses voltage deviation of the droop control to design the ETM, and proposes an optimal consensus algorithm for distributed energy resources. Further considering the economic operation, the work (Li et al., 2022) uses information of the voltage, power and increment cost to design the ETM, and presents a hierarchical and economic distributed ETC method for hybrid microgrids.

Although the aforementioned works have presented many useful results, there still exist the following limitations: (i) Although the PB disturbances exist in many practical systems, most works ignore their effects on the ETMs. Since the PB disturbances can seriously affect the state-related triggering thresholds of the SSRETMs (Peng et al., 2021; Shi et al., 2021; Li et al., 2022), especially during the steady-state response period, whether or not these SSRETMs still be effective becomes a question. Thus, it is necessary to design a novel ETM which is robust to PB disturbances. (ii) While most works focus on the ETM design to determine when to transmit data, what to transmit at the triggering instants has not drawn enough attention. However, for the widely used digital networks, it is difficult and unrealistic to transmit continuous-amplitude signals. Meanwhile, the quantization provides a solution for data communication in digital networks. (iii) When there exist the ETM and communication network in the sensor-to-controller channel, the premise mismatching problem between fuzzy plant and controller appears, which should be handled in the fuzzy control of DC microgrids. Thus, considering all the aforementioned attributing factors, it is a challenging task to model and analyse DC microgrids.

To overcome the limits above, this paper presents an event-driven fuzzy \mathcal{L}_∞ control strategy of DC microgrids, while addressing a variety of issues, including the dynamic ETM, FDI attacks, quantizer, PB disturbances, premise mismatching and delays. The main contributions are presented in the following. First, to overcome the limits of SSRETM (Li et al., 2022; Liu et al., 2021; Zhang and Zhang, 2022) that their triggering rate increases significantly when considering the PB disturbances, a dynamic ETM (DETM) is proposed, which is robust to the PB disturbances. Unlike continuous-time ETMs requiring complex Zeno-avoiding computation (Xing et al., 2021; Shafiee et al., 2021; Kang et al., 2022), the periodic DETM is naturally Zeno-free. Second, taking effects of the DETM, FDI attacks, quantizer, disturbances, premise mismatching and delays into account, a unified time-delay fuzzy system model of DC microgrids is established. Third, criteria for the GEUB stability in mean square with guaranteed \mathcal{L}_∞ -gain are derived, and the relationship between the ultimate bound of microgrid states and parameter of the DETM is established. Further, a fuzzy controller subject to mismatching premises is designed, which can achieve better control performance than the robust controller (Herrera et al., 2017).

Notations. *Col* and *diag* indicate the column matrix and diagonal matrix, respectively. I denotes the identity matrix, and $He\{A\}$ refers to $A + A^T$. λ_{min} indicates the minimum eigenvalue. \mathbb{N} is natural number set, \mathbb{Z} is integer set and \mathbb{R}^+ is nonnegative real number set. \mathbb{E} marks the mathematical expectation of a random variable. $\|\cdot\|$ denotes the Euclidean norm. $*$ refers to the symmetric item in a matrix, and \otimes marks the Kronecker product. Denote the number $M \times 10^N$ by MeN . For a signal $w(t)$, the \mathcal{L}_∞ -norm is defined as $\|w(t)\|_\infty = \text{ess sup}_{t \in \mathbb{R}^+} \|w(t)\|$.

System Modelling for the DC microgrid

System description

As shown in Figure 1, a DC microgrid contains Q CPL subsystems and a DC source subsystem. Sensors periodically sample voltage and current information. The DETM releases the sampled data only when the triggering condition is satisfied. The quantizer quantifies the released data of the DETM, and sends them to the event-triggered fuzzy quantized injection current (ETFQIC) controller. FDI attacks randomly inject false data in output signals of the controller.

Using Kirchhoff laws (Li et al., 2023a), and shifting the system equilibrium point to coordinate origin, the DC microgrid can be described as

$$\dot{\bar{x}}(t) = \bar{A}\bar{x}(t) - DH(\bar{x}(t)) + B_c \bar{v}_c(t) \quad (1)$$

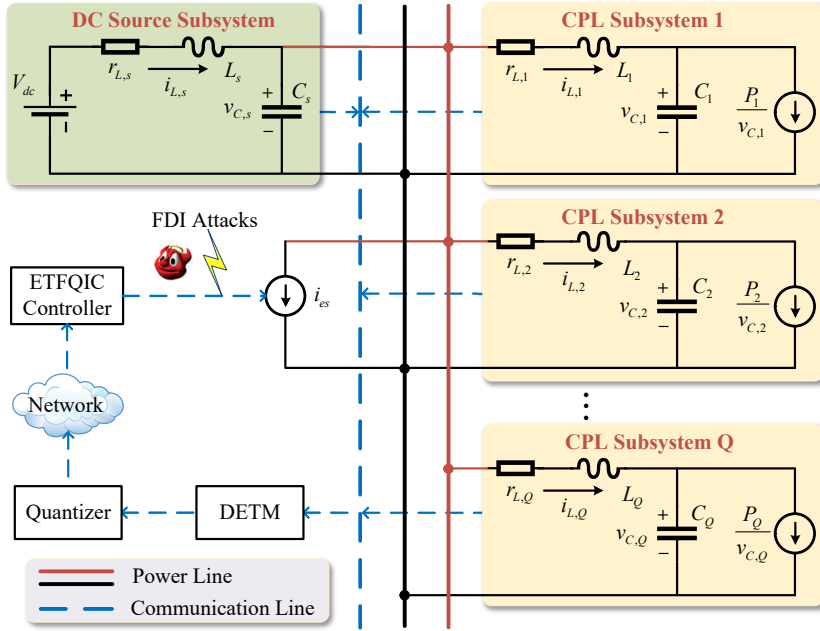


Figure 1. A DC microgrid with Q CPLs.

where $\bar{i}_c(t)$ is injection current, and

$$\left\{ \begin{array}{l} \bar{x}(t) = \begin{bmatrix} \bar{x}_1(t) \\ \vdots \\ \bar{x}_Q(t) \\ \bar{x}_s(t) \end{bmatrix}, H(\bar{x}(t)) = \begin{bmatrix} -h_1(\bar{x}_1(t)) \\ \vdots \\ -h_Q(\bar{x}_Q(t)) \end{bmatrix}, \bar{x}_s(t) = \begin{bmatrix} \bar{i}_{L,s} \\ \bar{v}_{C,s} \end{bmatrix} \\ \bar{x}_j(t) = \begin{bmatrix} \bar{i}_{L,j} \\ \bar{v}_{C,j} \end{bmatrix}, h_j(\bar{x}_j(t)) = \frac{\bar{v}_{C,j}}{v_{C_0,j}(\bar{v}_{C,j} + v_{C_0,j})}, j = 1, \dots, Q \end{array} \right.$$

$$\bar{A} = \begin{bmatrix} \bar{A}_1 & \dots & 0 & \bar{A}_{1s} \\ \vdots & \ddots & \vdots & \vdots \\ 0 & \dots & \bar{A}_Q & \bar{A}_{Qs} \\ \bar{A}_{cn} & \dots & \bar{A}_{cn} & \bar{A}_s \end{bmatrix}, D = \begin{bmatrix} d_1 & \dots & 0 \\ \vdots & \ddots & \vdots \\ 0 & \dots & d_Q \\ 0 & \dots & 0 \end{bmatrix}, B_c = \begin{bmatrix} 0 \\ \vdots \\ 0 \\ b_{es} \end{bmatrix}$$

$$\begin{cases} \bar{A}_j = \begin{bmatrix} -\frac{r_{L,j}}{L_j} & -\frac{1}{L_j} \\ \frac{1}{C_j} & 0 \end{bmatrix}, \bar{A}_{js} = \begin{bmatrix} 0 & \frac{1}{L_j} \\ 0 & 0 \end{bmatrix}, d_j = \begin{bmatrix} 0 \\ \frac{P_j}{C_j} \end{bmatrix}, j = 1, \dots, Q \\ \bar{A}_s = \begin{bmatrix} -\frac{r_s}{L_s} & -\frac{1}{L_s} \\ \frac{1}{C_s} & 0 \end{bmatrix}, \bar{A}_{cn} = \begin{bmatrix} 0 & 0 \\ -\frac{1}{C_s} & 0 \end{bmatrix}, b_{es} = \begin{bmatrix} 0 \\ -\frac{1}{C_s} \end{bmatrix} \end{cases}$$

where $L_j, C_j, r_{L,j}$ and $L_s, C_s, r_{L,s}$ denote the inductance, capacitance, resistance in the CPL subsystem and DC source subsystem, respectively. $v_{C,j}, v_{C,s}$ and $i_{L,j}, i_{L,s}$ refer to the corresponding capacitor voltages and inductor currents. $v_{C_0,j}$ is the operating point of the voltage $v_{C,j}$. P_j indicates the j th CPL's constant power, and V_{dc} denotes the DC source's voltage. Without losing generality (Vafamand et al., 2019), a DC microgrid containing one CPL is investigated.

For $\bar{v}_{C,1} \in [-\bar{v}_{C,1}^m, \bar{v}_{C,1}^m]$, the nonlinear term $h_1(\bar{x}_1(t))$ in (1) satisfies

$$\mathcal{K}_1 \bar{v}_{C,1} \leq h_1(\bar{x}_1(t)) \leq \mathcal{K}_2 \bar{v}_{C,1} \quad (2)$$

where $\mathcal{K}_1 = \frac{1}{v_{C_0,1}(\bar{v}_{C,1}^m + v_{C_0,1})}$ and $\mathcal{K}_2 = \frac{1}{v_{C_0,1}(-\bar{v}_{C,1}^m + v_{C_0,1})}$.

Using the sector nonlinearity method, it follows from (2) that

$$\begin{cases} h_1(\bar{x}_1(t)) = \mu_1(\bar{x}_1(t))\mathcal{K}_1 \bar{v}_{C,1} + \mu_2(\bar{x}_1(t))\mathcal{K}_2 \bar{v}_{C,1} \\ \mu_1(\bar{x}_1(t)) + \mu_2(\bar{x}_1(t)) = 1 \end{cases} \quad (3)$$

where membership functions $\mu_1(\bar{x}_1(t))$ and $\mu_2(\bar{x}_1(t))$ are derived as

$$\mu_1(\bar{x}_1(t)) = \frac{\mathcal{K}_2 \bar{v}_{C,1} - h_1(\bar{x}_1(t))}{(\mathcal{K}_2 - \mathcal{K}_1) \bar{v}_{C,1}}, \quad \mu_2(\bar{x}_1(t)) = \frac{h_1(\bar{x}_1(t)) - \mathcal{K}_1 \bar{v}_{C,1}}{(\mathcal{K}_2 - \mathcal{K}_1) \bar{v}_{C,1}} \quad (4)$$

Then, the fuzzy IF-THEN rules of the DC microgrid (1) can be described as follows.

Rule 1: if the premise variable $h_1(\bar{x}_1(t))/\bar{v}_{C,1}$ equals \mathcal{K}_1 , then $\dot{\bar{x}}(t) = A_1 \bar{x}(t) + B_c \bar{i}_c$.

Rule 2: if the premise variable $h_1(\bar{x}_1(t))/\bar{v}_{C,1}$ equals \mathcal{K}_2 , then $\dot{\bar{x}}(t) = A_2 \bar{x}(t) + B_c \bar{i}_c$.

where

$$A_i = \begin{bmatrix} \tilde{A}_i & \bar{A}_{1s} \\ \bar{A}_{cn} & \bar{A}_s \end{bmatrix}, \tilde{A}_1 = \begin{bmatrix} -\frac{r_{L,1}}{L_1} & -\frac{1}{L_1} \\ \frac{1}{C_1} & \frac{P_1}{C_1} \mathcal{K}_1 \end{bmatrix}, \tilde{A}_2 = \begin{bmatrix} -\frac{r_{L,1}}{L_1} & -\frac{1}{L_1} \\ \frac{1}{C_1} & \frac{P_1}{C_1} \mathcal{K}_2 \end{bmatrix}$$

Using membership functions (4), and considering the effect of noises, the fuzzy model of the DC microgrid (1) can be described as

$$\dot{\hat{x}}(t) = \sum_{i=1}^2 \mu_i \{A_i \bar{x}(t) + B_c \bar{v}_c + B_i^\omega \omega(t)\} \quad (5)$$

where $\omega(t)$ marks PB disturbances satisfying $\omega(t) \in \mathcal{L}_\infty$, A_i, B_c, B_i^ω are gain matrices, μ_i marks $\mu_i(\bar{x}_1(t))$.

Remark 1. *Unlike the work (Herrera et al., 2017) using a Lur'e system with disturbances to model the DC microgrid, this paper builds a T-S fuzzy model (5) of the DC microgrid. The comparison in simulation shows that the proposed fuzzy method performs better.*

Dynamic event-triggered communication mechanism

To reduce the unnecessary consumption of the limited system resources, a dynamic ETM is proposed as

$$d_{k+1}h = d_k h + \min\{ih \|\Theta^{0.5} \mathcal{D}\|^2 > \bar{\delta}(t)\}, \quad \bar{\delta}(t) = \delta_s(t) + \delta_d(t) + \delta_0 \quad (6)$$

where $i, k, d_k \in \mathbb{N}$, $\delta_s(t) = \delta_s \|\Theta^{0.5} \bar{x}(d_k h)\|^2$, $\delta_d(t) = [\frac{2}{\pi} \delta_d \arctan(\ell \|\mathcal{D}\|)] \|\Theta^{0.5} \bar{x}(d_k h)\|^2$, $\mathcal{D} = \bar{x}(d_k h) - \bar{x}(d_k h + ih)$, matrix $\Theta > 0$, scalars $\delta_s \geq 0, \delta_d \geq 0, \delta_0 \geq 0, \ell \geq 0$, $d_k h$ indicates the k_{th} triggering instant, and h is sampling period.

Unlike the periodic communication method (i.e., time-triggered mechanism (TTM)) releasing all the sampled data, the DETM (6) only releases data when the triggering condition is satisfied. Therefore, the triggering instants are a subset of the sampling instants, i.e., $\{\dots, d_k h, d_{k+1} h, \dots\} \subseteq \{\dots, ih, (i+1)h, \dots\}$. Unlike the continuous-time ETMs (Xing et al., 2021; Shafiee et al., 2021; Kang et al., 2022) which require complex analysis to ensure a positive minimum triggering interval (MTI), the DETM's MTI is lower bounded by the sampling period, and thus Zeno behavior (Li et al., 2023a) is naturally avoided. The Zeno-free idea comes from the works (Peng and Yang, 2013; Peng and Han, 2013).

Remark 2. *Unlike the SSRETMs (Li et al., 2022; Liu et al., 2021; Zhang and Zhang, 2022) which only use the static state-related threshold $\delta_s(t)$, the DETM's triggering threshold includes $\delta_s(t)$, a dynamic term $\delta_d(t)$ and a constant term δ_0 . During the transient period, the wildly fluctuating states often lead to a large $\delta_d(t)$. The resultant large triggering threshold help the DETM achieve larger triggering intervals than the SSRETMs. During the steady-state period, the small system states lead to a small threshold $\delta_s(t)$, which is seriously affected by the PB disturbances, and thus the triggering rate of the SSRETMs increases significantly. However, due to the constant threshold δ_0 which is not influenced by the disturbances, the*

DETM can still effectively reduce the triggering rate, which overcomes the limitation of the SSRETM. Besides, when $\delta_d(t) = \delta_0 = 0$, the DETM reduces to the SSRETM.

Signal quantization

While the DETM determines when to communicate, the quantizer determines what to communicate. To facilitate transmission of the triggered data in digital networks, a quantizer $f_{\bar{x}} = \text{col}\{f_{\bar{i}_{L,1}}, f_{\bar{v}_{C,1}}, f_{\bar{i}_{L,s}}, f_{\bar{v}_{C,s}}\}$ conducts quantization in each channel. Taking $f_{\bar{v}_{C,1}}$ for example, its quantization levels are described as

$$\{\pm \mathcal{Q}_{\bar{v}_{C,1}}^i \mid \mathcal{Q}_{\bar{v}_{C,1}}^i = \rho_{\bar{v}_{C,1}}^i \mathcal{Q}_{\bar{v}_{C,1}}^0, i \in \mathbb{Z}\} \cup \{0\} \quad (7)$$

where $\mathcal{Q}_{\bar{v}_{C,1}}^0 > 0$, and quantization density $\rho_{\bar{v}_{C,1}} \in (0, 1)$.

The logarithmic quantizer $f_{\bar{v}_{C,1}}$ is defined as

$$f_{\bar{v}_{C,1}} = \begin{cases} \mathcal{Q}_{\bar{v}_{C,1}}^i, & \text{if } \bar{v}_{C,1} \text{ is positive, } \bar{v}_{C,1} \in \mathcal{S}_{\bar{v}_{C,1}} \\ 0, & \text{if } \bar{v}_{C,1} \text{ is zero} \\ -f_{-\bar{v}_{C,1}}, & \text{if } \bar{v}_{C,1} \text{ is negative} \end{cases} \quad (8)$$

where $\mathcal{S}_{\bar{v}_{C,1}} = (\frac{1+\rho_{\bar{v}_{C,1}}}{2} \mathcal{Q}_{\bar{v}_{C,1}}^i, \frac{1+\rho_{\bar{v}_{C,1}}}{2\rho_{\bar{v}_{C,1}}} \mathcal{Q}_{\bar{v}_{C,1}}^i]$.

Based on the sector-bound expression method, using the same quantization density ρ in each channel, the quantized value of the triggered data $\bar{x}(d_k h)$ can be expressed as

$$\hat{x}(d_k h) = f_{\bar{x}(d_k h)} = (1 + \Delta_q) \bar{x}(d_k h) \quad (9)$$

where

$$\begin{cases} \hat{x}(d_k h) = \begin{bmatrix} \hat{x}_1(d_k h) \\ \hat{x}_s(d_k h) \end{bmatrix}, \hat{x}_1(d_k h) = \begin{bmatrix} \hat{i}_{L,1} \\ \hat{v}_{C,1} \end{bmatrix}, \hat{x}_s(d_k h) = \begin{bmatrix} \hat{i}_{L,s} \\ \hat{v}_{C,s} \end{bmatrix} \\ \Delta_q = I \otimes \Delta, \Delta \in [-\kappa, \kappa], \kappa = (1 - \rho)/(1 + \rho) \end{cases}$$

Closed-loop system modelling

Considering the transmission delay $\tau_k \in [\tilde{\tau}, \hat{\tau}]$ of the communication network in Figure 1, based on the triggering instants of the DETM, the controller's updating instants are described as $\{\dots, d_k h + \tau_k, d_{k+1} h + \tau_{k+1}, \dots\}$. Denoting $\nu_k = d_{k+1} - d_k - 1$, divide the updating interval $\mathcal{W}_k = [d_k h +$

$\tau_k, d_{k+1}h + \tau_{k+1})$ of the controller as

$$\mathcal{U}_k = \bigcup_{i_k=0}^{\nu_k} \mathcal{V}_{i_k}^{d_k}, \mathcal{V}_{i_k}^{d_k} = [d_k h + i_k h + \tau_k, \bar{\mathcal{V}}_{i_k}^{d_k}) \quad (10)$$

$$\text{where } \bar{\mathcal{V}}_{i_k}^{d_k} = \begin{cases} d_k h + (i_k + 1)h + \tau_k, & i_k = 0, 1, \dots, \nu_k - 1 \\ d_{k+1}h + \tau_{k+1}, & i_k = \nu_k \end{cases}.$$

On the subinterval $\mathcal{V}_{i_k}^{d_k}$, defining piecewise functions $\xi(t) = \bar{x}(d_k h) - \bar{x}(d_k h + i_k h)$ and $\phi(t) = t - (d_k h + i_k h)$, the quantized data in (9) can be expressed as

$$\hat{x}(d_k h) = (1 + \Delta_q)[\xi(t) + \bar{x}(t - \phi(t))] \quad (11)$$

Considering the premise mismatching issue, the ETFQIC controller is designed as

$$\hat{i}_c = \sum_{j=1}^2 \bar{\mu}_j K_j \hat{x}(d_k h), \quad t \in \phi_{\epsilon_k}^{d_k} \quad (12)$$

where $\bar{\mu}_1 = \frac{\mathcal{K}_2 \hat{v}_{C,1} - h_1(\hat{x}_1(d_k h))}{(\mathcal{K}_2 - \mathcal{K}_1) \hat{v}_{C,1}}$, $\bar{\mu}_2 = \frac{h_1(\hat{x}_1(d_k h)) - \mathcal{K}_1 \hat{v}_{C,1}}{(\mathcal{K}_2 - \mathcal{K}_1) \hat{v}_{C,1}}$, and $\bar{\mu}_j$ refers to $\bar{\mu}_j(\hat{x}(d_k h))$.

Remark 3. *Since there exist the DETM, quantizer and network delays between the microgrid and controller, the controller (12) can not share the same premise variables with the microgrid model (5). Instead, using the quantized value $\hat{x}(d_k h)$ of the DETM's triggered data, the controller's membership functions can be obtained. Namely, the premise mismatching issue is considered here, which is more reasonable and complex than the works (Mardani et al., 2019; Aslam et al., 2023) which assume the same premises in both of the plant and controller.*

Considering the FDI attacks in Figure 5, the control signal in (12) is randomly manipulated as

$$\bar{i}_c = \hat{i}_c + \beta(t)\mathcal{G}(t), \quad t \in \phi_{\epsilon_k}^{d_k} \quad (13)$$

where the injecting time of the attack signal $\mathcal{G}(t)$ follows a Bernoulli distribution $\beta(t) \in \{0, 1\}$ with $\mathbb{E}\{\beta(t)\} = \bar{\beta}$, and the controller output is attacked only when $\beta(t) = 1$. To improve the stealthy capacity of the FDI attacks, the attacker often limits the attacking energy as $\mathcal{G}^T(t)\mathcal{G}(t) \leq \hat{i}_c^T G^T \hat{i}_c$ with a bounded matrix G .

Using the DC microgrid (5) and the attacked control signal (13), the T-S fuzzy system model is established as

$$\begin{aligned} \dot{\bar{x}}(t) = & \sum_{i=1}^2 \sum_{j=1}^2 \mu_i \bar{\mu}_j \{A_i \bar{x}(t) + B_c K_j (1 + \Delta_q) [\xi(t) \\ & + \bar{x}(t - \phi(t))] + B_c \beta(t) \mathcal{G}(t) + B_i^\omega \omega(t)\} \end{aligned} \quad (14)$$

where a performance variable $z(t) = \sum_{i=1}^2 C_i \bar{x}(t)$ with gain matrix C_i is introduced to analyse the disturbance rejection performance.

Stability analysis

Definition 1. (Zou et al., 2017) For a system with state $x(t)$ and initial condition $x(0)$, if there exist scalars $a_1, a_2, a_3 > 0$ satisfying

$$\mathbb{E}\{\|x(t)\|^2\} \leq a_1 \|x(0)\|^2 e^{-a_2 t} + a_3, \quad \forall t \geq 0 \quad (15)$$

then, the system is globally exponentially ultimately bounded in mean square.

Definition 2. (Donkers and Heemels, 2012) For a system with disturbances satisfying $\omega(t) \in \mathcal{L}_\infty$, the \mathcal{L}_∞ -gain is defined as

$$\bar{\zeta} = \inf\{\zeta \in \mathbb{R}^+ | \exists \varrho : \mathcal{X} \rightarrow \mathbb{R}^+, \text{ such that } \|z\|_\infty \leq \zeta \|\omega\|_\infty + \varrho(x(0))\} \quad (16)$$

where $x(0) \in \mathcal{X}$ is initial states, and \mathcal{X} refers to the system state set.

Theorem 1. For sampling period $h > 0$, the DETM parameters $\delta_s \geq 0, \delta_d \geq 0, \delta_0 \geq 0$, quantisation parameters $\rho \in (0, 1)$ and Δ_q , attacking parameters $\bar{\beta} \in [0, 1]$ and G , delay parameters $\hat{\tau} > \check{\tau} > 0$, disturbance parameters $\zeta^2 > \gamma > 0$, scalar $\sigma > 0$, $\alpha_i > 0$ satisfying $\bar{\mu}_i \geq \alpha_i \mu_i$ ($i = 1, 2$), if there exist

matrices $U > 0, P > 0, R > 0, H_1 > 0, H_2 > 0, \Theta > 0, \Lambda^1, \Lambda^2$ and M satisfying $\begin{bmatrix} H_2 & * \\ W & H_2 \end{bmatrix} > 0$ and

$$\Phi^{ij} - \Lambda^i < 0, 1 \leq i, j \leq 2 \quad (17)$$

$$\alpha_i(\Phi^{ii} - \Lambda^i) + \Lambda^i < 0, i = 1, 2 \quad (18)$$

$$\alpha_j(\Phi^{ij} - \Lambda^i) + \alpha_i(\Phi^{ji} - \Lambda^j) + \Lambda^i + \Lambda^j < 0, 1 \leq i < j \leq 2 \quad (19)$$

$$\begin{bmatrix} \sigma P - C_i^T C_i & * \\ 0 & \zeta^2 - \gamma \end{bmatrix} \geq 0, i = 1, 2 \quad (20)$$

where

$$\begin{aligned} \Phi^{ij} &= \Upsilon^{ij} + \delta(\mathcal{S}_3 + \mathcal{S}_5)^T \Theta (\mathcal{S}_3 + \mathcal{S}_5) - \mathcal{S}_5^T \Theta \mathcal{S}_5 - \bar{\beta} \mathcal{S}_6^T \mathcal{S}_6 - \gamma \mathcal{S}_7^T \mathcal{S}_7 \\ &\quad + \bar{\beta} (K_j(1 + \Delta_q)(\mathcal{S}_3 + \mathcal{S}_5))^T G^T G (K_j(1 + \Delta_q)(\mathcal{S}_3 + \mathcal{S}_5)) \\ \Upsilon^{ij} &= \sigma \mathcal{S}_1^T P \mathcal{S}_1 + He\{\mathcal{S}_1^T P \Psi_1^{ij}\} - e^{-\sigma \phi_1} \mathcal{S}_2^T R \mathcal{S}_2 + \Psi_1^{ijT} (\phi_1^2 H_1 + \phi_{21}^2 H_2) \Psi_1^{ij} \\ &\quad + \bar{\beta}^2 \Psi_2^T (\phi_1^2 H_1 + \phi_{21}^2 H_2) \Psi_2 - e^{-\sigma \phi_1} (\mathcal{S}_1 - \mathcal{S}_2)^T H_1 (\mathcal{S}_1 - \mathcal{S}_2) + \mathcal{S}_1^T R \mathcal{S}_1 \\ &\quad - e^{-\sigma \phi_2} (\mathcal{S}_2 - \mathcal{S}_3)^T H_2 (\mathcal{S}_2 - \mathcal{S}_3) + e^{-\sigma \phi_1} \mathcal{S}_2^T U \mathcal{S}_2 - e^{-\sigma \phi_2} \mathcal{S}_4^T U \mathcal{S}_4 \\ &\quad - e^{-\sigma \phi_2} (\mathcal{S}_3 - \mathcal{S}_4)^T H_2 (\mathcal{S}_3 - \mathcal{S}_4) - e^{-\sigma \phi_2} He\{(\mathcal{S}_3 - \mathcal{S}_4)^T W (\mathcal{S}_2 - \mathcal{S}_3)\} \\ \Psi_1^{ij} &= A_i \mathcal{S}_1 + B_c K_j (1 + \Delta_q) (\mathcal{S}_3 + \mathcal{S}_5) + \bar{\beta} B_c \mathcal{S}_6 + B_i^\omega \mathcal{S}_7, \\ \Psi_2 &= B_c \mathcal{S}_6, \delta = \delta_s + \delta_d, \bar{\beta} = (\bar{\beta}(1 - \bar{\beta}))^{0.5}, \\ \mathcal{S}_i &= [\underbrace{0 \dots 0}_{i-1} \ I \ \underbrace{0 \dots 0}_{7-i}], \quad i = 1, \dots, 7 \end{aligned}$$

then, the DC microgrid (14) subject to the dynamic ETM, FDI attacks, quantizer, PB disturbances, premise mismatching and network delays is GEUB in mean square, and the \mathcal{L}_∞ -gain is smaller than or equal to ζ .

Proof. Construct a Lyapunov functional as

$$\begin{aligned} V(t) &= \bar{x}^T(t) P \bar{x}(t) + \int_{t-\phi_1}^t e^{\sigma(\vartheta-t)} \bar{x}^T(\vartheta) R \bar{x}(\vartheta) d\vartheta \\ &\quad + \int_{t-\phi_2}^{t-\phi_1} e^{\sigma(\vartheta-t)} \bar{x}^T(\vartheta) U \bar{x}(\vartheta) d\vartheta \\ &\quad + \sum_{i=1}^2 \phi_{i(i-1)} \int_{-\phi_i}^{-\phi_{i-1}} \int_{t+\theta}^t e^{\sigma(\vartheta-t)} \dot{\bar{x}}^T(\vartheta) H_i \dot{\bar{x}}(\vartheta) d\vartheta d\theta \end{aligned} \quad (21)$$

where $\phi_{i(i-1)} = \phi_i - \phi_{i-1}$, $\phi_0 = 0$, $\phi_1 = \tilde{\tau}$ and $\phi_2 = h + \hat{\tau}$.

Taking the derivative of $V(t)$ yields

$$\begin{aligned} \dot{V}(t) &\leq -\sigma V(t) + \sigma \bar{x}^T(t) P \bar{x}(t) + H e \{ \bar{x}^T(t) P \dot{\bar{x}}(t) \} + \bar{x}^T(t) R \bar{x}(t) \\ &\quad - e^{-\sigma \phi_1} \bar{x}^T(t - \phi_1) R \bar{x}(t - \phi_1) + e^{-\sigma \phi_1} \bar{x}^T(t - \phi_1) U \bar{x}(t - \phi_1) \\ &\quad - e^{-\sigma \phi_2} \bar{x}^T(t - \phi_2) U \bar{x}(t - \phi_2) + \dot{\bar{x}}^T(t) (\phi_1^2 H_1 + \phi_{21}^2 H_2) \dot{\bar{x}}(t) \\ &\quad - \phi_1 e^{-\sigma \phi_1} \int_{t-\phi_1}^t \dot{\bar{x}}^T(\theta) H_1 \dot{\bar{x}}(\theta) d\theta - \phi_{21} e^{-\sigma \phi_2} \int_{t-\phi_2}^{t-\phi_1} \dot{\bar{x}}^T(\theta) H_2 \dot{\bar{x}}(\theta) d\theta \end{aligned} \quad (22)$$

Similar to (Li et al., 2023a), use reciprocally convex method (Naami et al., 2022) and Jensen inequality (Zhang et al., 2023) to handle the integral terms in (22). Then, considering effects of the DETM, FDI attacks and PB disturbances, we have

$$\begin{aligned} &\mathbb{E}\{\dot{V}(t)\} + \sigma \mathbb{E}\{V(t)\} \\ &\leq \sum_{i=1}^2 \sum_{j=1}^2 \mu_i \bar{\mu}_j \chi^T(t) \Upsilon^{ij} \chi(t) - \xi^T(t) \Theta \xi(t) + \delta \mathcal{H}_2^T \Theta \mathcal{H}_2 + \delta_0 \\ &\quad - \bar{\beta} \mathcal{G}^T(t) \mathcal{G}(t) + \bar{\beta} \mathcal{H}_1^T G^T G \mathcal{H}_1 - \gamma \omega^T(t) \omega(t) + \gamma \omega^T(t) \omega(t) \\ &\leq \sum_{i=1}^2 \sum_{j=1}^2 \mu_i \bar{\mu}_j \chi^T(t) \Phi^{ij} \chi(t) + \gamma \|\omega(t)\|_\infty^2 + \delta_0 \end{aligned} \quad (23)$$

where $\chi(t) = \text{col}\{\bar{x}(t), \bar{x}(t - \phi_1), \bar{x}(t - \phi(t)), \bar{x}(t - \phi_2), \xi(t), \mathcal{G}(t), \omega(t)\}$, $\mathcal{H}_1 = K_j(1 + \Delta_q) \mathcal{H}_2$ and $\mathcal{H}_2 = \bar{x}(t - \phi(t)) + \xi(t)$.

Using the method in (Peng et al. (2017)) to handle the premise mismatching problem, and designing a zero-value term $\sum_{i=1}^2 \sum_{j=1}^2 \mu_i (\mu_j - \bar{\mu}_j) \chi^T(t) \Lambda^i \chi(t) = 0$, the following equation holds

$$\begin{aligned} \sum_{i=1}^2 \sum_{j=1}^2 \mu_i \bar{\mu}_j \chi^T(t) \Phi^{ij} \chi(t) &= \sum_{i=1}^2 \sum_{j=1}^2 \mu_i \bar{\mu}_j \chi^T(t) \Phi^{ij} \chi(t) + \sum_{i=1}^2 \sum_{j=1}^2 \mu_i (\mu_j - \bar{\mu}_j) \chi^T(t) \Lambda^i \chi(t) \\ &= \sum_{i=1}^2 \sum_{j=1}^2 \mu_i \bar{\mu}_j \chi^T(t) (\Phi^{ij} - \Lambda^i) \chi(t) + \sum_{i=1}^2 \sum_{j=1}^2 \mu_i \mu_j \chi^T(t) \Lambda^i \chi(t) \end{aligned} \quad (24)$$

Using the conditions (17) and $\bar{\mu}_j \geq \alpha_j \mu_j$ in Theorem 1, it follows from (24) that

$$\begin{aligned}
\sum_{i=1}^2 \sum_{j=1}^2 \mu_i \bar{\mu}_j \chi^T(t) \Phi^{ij} \chi(t) &\leq \sum_{i=1}^2 \sum_{j=1}^2 \mu_i \mu_j \chi^T(t) \{\alpha_j (\Phi^{ij} - \Lambda^i) + \Lambda^i\} \chi(t) \\
&\leq \sum_{i=1}^2 \mu_i \mu_i \chi^T(t) \{\alpha_i (\Phi^{ii} - \Lambda^i) + \Lambda^i\} \chi(t) \\
&\quad + \sum_{i=1}^2 \sum_{j>i}^2 \mu_i \mu_j \chi^T(t) \{\alpha_j (\Phi^{ij} - \Lambda^i) \\
&\quad + \alpha_i (\Phi^{ji} - \Lambda^j) + \Lambda^i + \Lambda^j\} \chi(t)
\end{aligned} \tag{25}$$

Substituting (18) and (19) into (25), we have $\sum_{i=1}^2 \sum_{j=1}^2 \mu_i \bar{\mu}_j \chi^T(t) \Phi^{ij} \chi(t) \leq 0$. Using this inequality, it follows from (23) that

$$\mathbb{E}\{V(t)\} \leq e^{-\sigma t} \mathbb{E}\{V(0)\} + \sigma^{-1} (1 - e^{-\sigma t}) (\gamma \|\omega(t)\|_\infty^2 + \delta_0) \tag{26}$$

For stability analysis with $\omega(t) = 0$, one derives from (26) that

$$\begin{cases} \mathbb{E}\{\|\bar{x}(t)\|^2\} \leq \mathcal{B}, \mathcal{B} = \lambda_{\min}^{-1}\{P\} \mathbb{E}\{V(0)\} e^{-\sigma t} + \mathcal{B}_\infty \\ \mathcal{B}_\infty = \lim_{t \rightarrow \infty} \mathcal{B} = \lambda_{\min}^{-1}\{P\} \sigma^{-1} \delta_0 \end{cases} \tag{27}$$

where \mathcal{B} and \mathcal{B}_∞ are called exponential bound and ultimate bound, respectively. According to Definition 1, the system (14) is GEUB in mean square.

Next, the disturbance rejection performance is investigated. Using $\text{col}\{\bar{x}(t), \omega(t)\}$ to pre- and post-multiply (20) yields

$$z^T(t) z(t) \leq \sigma \bar{x}^T(t) P \bar{x}(t) + (\zeta^2 - \gamma) \omega^T(t) \omega(t) \leq \sigma \mathbb{E}\{V(t)\} + (\zeta^2 - \gamma) \|\omega(t)\|_\infty^2 \tag{28}$$

Using (26), it follows from (28) that

$$z^T(t) z(t) \leq \zeta^2 \|\omega(t)\|_\infty^2 + \sigma \mathbb{E}\{V(0)\} + \delta_0 \Rightarrow \|z(t)\|_\infty \leq \zeta \|\omega(t)\|_\infty + \varrho(\bar{x}(0)) \tag{29}$$

where $\varrho(\bar{x}(0)) = (\sigma \mathbb{E}\{V(0)\} + \delta_0)^{0.5}$. According to Definition 2, the \mathcal{L}_∞ gain of the system (14) is smaller than or equal to ζ . This completes the proof.

Remark 4. For the DETM (6), its parameters (δ_s, δ_d) affect feasibility of the linear matrix inequality (LMIs) in Theorem 1, while the parameter δ_0 influences the ultimate bound \mathcal{B}_∞ of system states in (27). A larger δ_0 results in a lower triggering rate of the DETM but a larger size of the ultimate bound \mathcal{B}_∞ . Thus, by choosing δ_0 , tradeoffs can be made between communication and control performances.

In Theorem 1, controller gain $K_j(j = 1, 2)$, Lyapunov functional parameters (P, H_1, H_2) and quantizer parameter Δ_q are coupled. Therefore, the next section will present a controller design method.

Controller design

Lemma 1. (Zhang et al., 2021) For symmetric matrix Γ_1 , matrices Γ_2 and Γ_3 , if there exists $\vartheta > 0$ satisfying

$$\Gamma_1 + \vartheta \Gamma_2^T \Gamma_2 + \vartheta^{-1} \Gamma_3^T \Gamma_3 < 0 \quad (30)$$

then, for \mathcal{J} satisfying $\mathcal{J}^T \mathcal{J} \leq I$, the following inequality holds

$$\Gamma_1 + \Gamma_2^T \mathcal{J} \Gamma_3 + \Gamma_3^T \mathcal{J}^T \Gamma_2 < 0 \quad (31)$$

Lemma 2. (Li et al., 2023b) For a positive definite matrix $\mathcal{C} > 0$ and a symmetric matrix M , there exists $\epsilon > 0$ such that

$$-M\mathcal{C}^{-1}M \leq \epsilon^2\mathcal{C} - 2\epsilon M \quad (32)$$

Lemma 3. (Schur complement lemma) (Duan and Yu, 2013) For a symmetric partitioned matrix

$$S = \begin{bmatrix} S_{11} & S_{12} \\ S_{12}^T & S_{22} \end{bmatrix}, S < 0 \text{ is equivalent to}$$

$$S_{11} < 0, S_{22} - S_{12}^T S_{11}^{-1} S_{12} < 0 \quad (33)$$

$$\text{or } S_{22} < 0, S_{11} - S_{12} S_{22}^{-1} S_{12}^T < 0 \quad (34)$$

Theorem 2. For sampling period $h > 0$, delay parameters $\hat{\tau} > \tilde{\tau} > 0$, DETM parameters $\delta_s \geq 0, \delta_d \geq 0, \delta_0 \geq 0$, quantisation density $\rho \in (0, 1)$, attacking parameters $\bar{\beta} \in [0, 1]$ and G , disturbance parameters $\zeta^2 > \gamma > 0$, scalar $\sigma > 0, \alpha_j$ satisfying $\bar{\mu}_j \geq \alpha_j \mu_j (j = 1, 2)$, if there exist matrices $\bar{U} > 0, X > 0, \bar{R} >$

$0, \bar{H}_1 > 0, \bar{H}_2 > 0, \bar{\Theta} > 0, \bar{\Lambda}^1, \bar{\Lambda}^2, Y_1, Y_2$ and \bar{W} such that $\begin{bmatrix} \bar{H}_2 & * \\ \bar{W} & \bar{H}_2 \end{bmatrix} > 0$ and

$$\mathcal{L}^{ij} < 0, 1 \leq i, j \leq 2 \quad (35)$$

$$\alpha_i \bar{\mathcal{L}}^{ii} < 0, i = 1, 2 \quad (36)$$

$$\alpha_j \bar{\mathcal{L}}^{ij} + \alpha_i \bar{\mathcal{L}}^{ji} < 0, 1 \leq i < j \leq 2 \quad (37)$$

$$\begin{bmatrix} \sigma X & * & * \\ 0 & \zeta^2 - \gamma & * \\ C_i X & 0 & I \end{bmatrix} \geq 0, i = 1, 2 \quad (38)$$

where $\bar{\mathcal{L}}^{ij} = \mathcal{L}^{ij} + a_j^{-1} \bar{\Lambda}^i$ and

$$\mathcal{L}^{ij} = \begin{bmatrix} \mathcal{L}_{11}^{ij} & * & * \\ \mathcal{L}_{21}^j & \mathcal{L}_{22} & * \\ \mathcal{L}_{31} & 0 & \mathcal{L}_{33} \end{bmatrix}, \mathcal{L}_{11}^{ij} = \begin{bmatrix} \bar{\mathcal{Q}}_{11}^{ij} & * & * & * \\ \bar{\mathcal{Q}}_{21}^{ij} & \bar{\mathcal{Q}}_{22} & * & * \\ \bar{\mathcal{Q}}_{31} & 0 & \bar{\mathcal{Q}}_{33} & * \\ \bar{\mathcal{Q}}_{41}^j & 0 & 0 & \bar{\mathcal{Q}}_{44} \end{bmatrix},$$

$$\bar{\mathcal{Q}}_{11}^{ij} = \begin{bmatrix} \mathcal{T}_{11}^i & * & * & * & * & * & * \\ \mathcal{T}_{21} & \mathcal{T}_{22} & * & * & * & * & * \\ \mathcal{T}_{31}^j & \mathcal{T}_{32} & \mathcal{T}_{33} & * & * & * & * \\ 0 & \mathcal{T}_{42} & \mathcal{T}_{43} & \mathcal{T}_{44} & * & * & * \\ \mathcal{T}_{51}^j & 0 & 0 & 0 & \mathcal{T}_{55} & * & * \\ \mathcal{T}_{61} & 0 & 0 & 0 & 0 & \mathcal{T}_{66} & * \\ \mathcal{T}_{71}^i & 0 & 0 & 0 & 0 & 0 & \mathcal{T}_{77} \end{bmatrix}$$

$$\mathcal{L}_{21}^j = \kappa [(B_c Y_j)^T \overbrace{0 \dots 0}^6 \phi_1 (B_c Y_j)^T \phi_{21} (B_c Y_j)^T 0 0 0 (G Y_j)^T],$$

$$\mathcal{L}_{22} = \varepsilon_q^2 \varepsilon_q^{-1} I - 2\varepsilon_q X, \mathcal{L}_{31} = [0 0 X 0 X \overbrace{0 \dots 0}^8], \mathcal{L}_{33} = -\varepsilon_q^{-1},$$

$$\bar{\mathcal{Q}}_{21}^{ij} = \begin{bmatrix} \phi_1 \mathcal{Z}_1 \\ \phi_{21} \mathcal{Z}_1 \end{bmatrix}, \mathcal{Z}_1 = [A_i X 0 B_c Y_j 0 B_c Y_j \bar{\beta} B_c B_i^w],$$

$$\bar{\mathcal{Q}}_{22} = \text{diag}\{\varepsilon_1^2 H_1 - 2\varepsilon_1 X, \varepsilon_2^2 H_2 - 2\varepsilon_2 X\}, \bar{\mathcal{Q}}_{33} = \text{diag}\{\varepsilon_3^2 H_1 - 2\varepsilon_3 X, \varepsilon_4^2 H_2 - 2\varepsilon_4 X\},$$

$$\bar{\mathcal{Q}}_{31} = \tilde{\beta} \begin{bmatrix} \phi_1 \mathcal{Z}_2 \\ \phi_{21} \mathcal{Z}_2 \end{bmatrix}, \mathcal{Z}_2 = [0 0 0 0 0 B_c 0], \bar{\mathcal{Q}}_{41}^j = \begin{bmatrix} \delta^{0.5} X \mathcal{Z}_3 \\ G Y_j \mathcal{Z}_3 \end{bmatrix}, \mathcal{Z}_3 = [0 0 I 0 I 0 0],$$

$$\bar{\mathcal{Q}}_{44} = \text{diag}\{\varepsilon_5^2 \bar{\Theta} - 2\varepsilon_5 X, -\bar{\beta}^{-1}\}, \mathcal{T}_{11}^i = \sigma X + \bar{R} + \text{He}\{A_i X\} - e^{-\sigma \phi_1} \bar{H}_1, \mathcal{T}_{21} = e^{-\sigma \phi_1} \bar{H}_1,$$

$$\mathcal{T}_{22} = e^{-\sigma \phi_1} (\bar{U} - \bar{R} - \bar{H}_1) - e^{-\sigma \phi_2} \bar{H}_2, \mathcal{T}_{31}^j = (B_c Y_j)^T, \mathcal{T}_{32} = e^{-\sigma \phi_2} (\bar{H}_2 - \bar{W}),$$

$\mathcal{T}_{33} = e^{-\sigma\phi_2}(\bar{W} + \bar{W}^T - 2\bar{H}_2)$, $\mathcal{T}_{42} = e^{-\sigma\phi_2}\bar{W}$, $\mathcal{T}_{43} = e^{-\sigma\phi_2}(\bar{H}_2 - \bar{W})$,
 $\mathcal{T}_{44} = -e^{-\sigma\phi_2}(\bar{U} + \bar{H}_2)$, $\mathcal{T}_{51}^j = (B_c Y_j)^T$, $\mathcal{T}_{55} = -\bar{\Theta}$,
 $\mathcal{T}_{61} = \bar{\beta} B_c^T$, $\mathcal{T}_{66} = -\bar{\beta}$, $\mathcal{T}_{71}^i = B_i^{\omega T}$, $\mathcal{T}_{77} = -\gamma$,
 $\bar{R} = X R X$, $\bar{U} = X U X$, $\bar{W} = X W X$, $\bar{H}_i = X H_i X$, $\bar{\Lambda}^i = \Pi \Lambda^i \Pi$, ($i = 1, 2$),
 $\Pi = \text{diag}\{X, X, X, X, X, I, I\}$, $\bar{\Theta} = X \Theta X$, $Y_j = K_j X$ ($j = 1, 2$),
then, the DC microgrid (14) is GEUB in mean square with guaranteed \mathcal{L}_∞ -gain. Besides, the controller gain ($K_j = Y_j X^{-1}$, $j = 1, 2$) and the DETM parameter ($\Theta = X^{-1} \bar{\Theta} X^{-1}$) can be computed.

Proof. From (17), one derives

$$\Phi^{ij} - \Lambda^i = \mathcal{Q}^{ij} + He\{L_{q1}^{jT} \Delta_q(t) L_{q2}\} < 0 \quad (39)$$

where $L_{q1}^j = [\mathcal{S}_1^T P B_c K_j \ \phi_1 B_c K_j \ \phi_{21} B_c K_j \ 0 \ 0 \ 0 \ G K_j]^T$, $L_{q2} = \mathcal{S}_3 + \mathcal{S}_5$,

$$\begin{aligned}
\mathcal{Q}_{11}^{ij} &= \sigma \mathcal{S}_1^T P \mathcal{S}_1 + He\{\mathcal{S}_1^T P \tilde{\Psi}_1^{ij}\} - e^{-\sigma\phi_1} \mathcal{S}_2^T R \mathcal{S}_2 - e^{-\sigma\phi_1} (\mathcal{S}_1 - \mathcal{S}_2)^T H_1 (\mathcal{S}_1 - \mathcal{S}_2) \\
&+ \mathcal{S}_1^T R \mathcal{S}_1 - e^{-\sigma\phi_2} (\mathcal{S}_2 - \mathcal{S}_3)^T H_2 (\mathcal{S}_2 - \mathcal{S}_3) + e^{-\sigma\phi_1} \mathcal{S}_2^T U \mathcal{S}_2 \\
&- e^{-\sigma\phi_2} (\mathcal{S}_3 - \mathcal{S}_4)^T H_2 (\mathcal{S}_3 - \mathcal{S}_4) - e^{-\sigma\phi_2} \mathcal{S}_4^T U \mathcal{S}_4 - e^{-\sigma\phi_2} He\{(\mathcal{S}_3 - \mathcal{S}_4)^T M (\mathcal{S}_2 - \mathcal{S}_3)\} \\
&- \mathcal{S}_5^T \Theta \mathcal{S}_5 - \bar{\beta} \mathcal{S}_6^T \mathcal{S}_6 - \gamma \mathcal{S}_7^T \mathcal{S}_7 - \Lambda^i,
\end{aligned}$$

$$\begin{aligned}
\mathcal{Q}_{21}^{ij} &= \begin{bmatrix} \phi_1 \tilde{\Psi}_1^{ij} \\ \phi_{21} \tilde{\Psi}_1^{ij} \end{bmatrix}, \quad \mathcal{Q}_{31} = \tilde{\beta} \begin{bmatrix} \phi_1 \Psi_2 \\ \phi_{21} \Psi_2 \end{bmatrix}, \quad \mathcal{Q}_{41}^j = \begin{bmatrix} \delta^{0.5} (\mathcal{S}_3 + \mathcal{S}_5) \\ G K_j (\mathcal{S}_3 + \mathcal{S}_5) \end{bmatrix}, \quad \mathcal{Q}_{44} = \begin{bmatrix} -\Theta^{-1} & * \\ 0 & -\bar{\beta}^{-1} \end{bmatrix}, \\
\mathcal{Q}_{22} = \mathcal{Q}_{33} &= \text{diag}\{-H_1^{-1}, -H_2^{-1}\}, \quad \tilde{\Psi}_1^{ij} = A_i \mathcal{S}_1 + B_c K_j (\mathcal{S}_3 + \mathcal{S}_5) + \bar{\beta} B_c \mathcal{S}_6 + B_i^\omega \mathcal{S}_7,
\end{aligned}$$

According to Lemma 1, (39) holds if the following inequality is satisfied

$$\mathcal{Q}^{ij} + \epsilon_q^{-1} \kappa^2 L_{q1}^{jT} L_{q1}^j + \epsilon_q L_{q2}^T L_{q2} < 0 \quad (40)$$

Applying Lemma 3 (Schur complement lemma) to (40) yields

$$\mathcal{P}^{ij} = \begin{bmatrix} \mathcal{Q}^{ij} & * & * \\ \kappa L_{q1}^j & -\epsilon_q & * \\ L_{q2} & 0 & -\epsilon_q^{-1} \end{bmatrix} < 0 \quad (41)$$

Define $\Upsilon = \text{diag}\{\underbrace{X, \dots, X}_5, \underbrace{I, \dots, I}_8, X, I\}$ and $X = P^{-1}$, it follows from (41) that

$$\mathcal{L}^{ij} = \Upsilon \mathcal{P}^{ij} \Upsilon < 0 \quad (42)$$

where

$$\left\{ \begin{array}{l} \check{\mathcal{L}}^{ij} = \begin{bmatrix} \check{\mathcal{L}}_{11}^{ij} & * & * \\ \check{\mathcal{L}}_{21}^j & \check{\mathcal{L}}_{22} & * \\ \check{\mathcal{L}}_{31} & 0 & \check{\mathcal{L}}_{33} \end{bmatrix}, \check{\mathcal{L}}_{11}^{ij} = \begin{bmatrix} \check{\mathcal{Q}}_{11}^{ij} & * & * & * \\ \check{\mathcal{Q}}_{21}^{ij} & \check{\mathcal{Q}}_{22} & * & * \\ \check{\mathcal{Q}}_{31} & 0 & \check{\mathcal{Q}}_{33} & * \\ \check{\mathcal{Q}}_{41}^j & 0 & 0 & \check{\mathcal{Q}}_{44} \end{bmatrix} \\ \check{\mathcal{Q}}_{22} = \check{\mathcal{Q}}_{33} = \text{diag}\{-X\bar{H}_1^{-1}X, -X\bar{H}_2^{-1}X\} \\ \check{\mathcal{Q}}_{44} = \text{diag}\{-X\bar{\Theta}^{-1}X, -\bar{\beta}^{-1}\}, \check{\mathcal{L}}_{22} = -\epsilon_q XX \end{array} \right.$$

Using Lemma 3 to handle the nonlinear terms $\check{\mathcal{L}}_{22}$, $\check{\mathcal{Q}}_{22}$, $\check{\mathcal{Q}}_{33}$ and $\check{\mathcal{Q}}_{44}$, (35) is obtained. Similarly, (36) and (37) can be derived from (18) and (19), respectively. Besides, applying Schur complement to (20), and using matrix $\text{diag}\{X, I, I\}$ to handle the result, (38) can be achieved. The proof is thus completed.

Remark 5. Compared with the emulation method (Wang et al., 2020) which first designs a controller using traditional methods, and then designs the ETM using the given controller, Theorem 2 can simultaneously compute the DETM parameter $\Theta = X^{-1}\bar{\Theta}X^{-1}$ and the controller gains $K_j = Y_j X^{-1}$ ($j = 1, 2$), which is more convenient.

Case studies

DC microgrid example

Table 1. DC microgrid with one CPL.

$r_1 = 1.1\Omega$	$C_s = 500\sigma F$	$v_{C_{0,1}} = 196.64V$
$L_1 = 39.5mH$	$r_s = 1.1\Omega$	$V_{dc} = 200V$
$C_1 = 500\sigma F$	$L_s = 39.5mH$	$P_1 = 300W$

Use the DC microgrid in Table 1 (Mardani et al., 2019) for example. Other parameters are set as: the FDI signal $\mathcal{G}(t) = -\tanh(0.8\hat{i}_{es})$ with attack expectation $\bar{\beta} = 0.1$, the DETM parameters $\delta_s = 1.6e - 4$, $\delta_d = 2.4e - 4$, $\delta_0 = 7e - 5$, $\ell = 50$, quantisation density $\rho = 0.923$, PB disturbances $\omega(t) = \sin(2\pi 100t)$ and the related parameters $\gamma = 1$, $\zeta = 1.03$, $B_i^\omega = \text{col}\{1, 1, 0, 0\}$ and $C_i = \text{col}\{0, 0.01, 0, 0\}$, premise mismatching scalars $\alpha_1 = 0.9$, $\alpha_2 = 0.8$, sampling period $h = 0.1ms$, delays bounds $\tilde{\tau} = 0.01ms$, $\hat{\tau} = 0.02ms$, decay rate $\sigma = 3$, and the initial states $\text{col}\{19, -30, 19, -30\}$.

Using the linear matrix inequalities in Theorem 2, the ETFQIC controller (12) and the dynamic ETM (6) can be designed as

$$\begin{cases} K_1 = \begin{bmatrix} 4.1732 & 0.1833 & 0.4776 & 0.5389 \end{bmatrix} \\ K_2 = \begin{bmatrix} 4.1491 & 0.1903 & 0.4824 & 0.5389 \end{bmatrix} \end{cases} \quad (43)$$

$$\Theta = \begin{bmatrix} 1707 & 77.60 & 181.3 & 110.8 \\ 77.60 & 15.99 & 1.292 & 4.798 \\ 181.3 & 1.292 & 145.1 & 12.01 \\ 110.8 & 4.798 & 12.01 & 14.21 \end{bmatrix} \quad (44)$$

As shown in Figure 2 (a), for the unstable microgrid in open loop, considering effects of the DETM, FDI attacks, quantizer, PB disturbances, premise mismatching and delays, the ETFQIC controller (43) can still stabilize the system. Besides, the capacitor voltage $v_{C,1}$ and inductor current $i_{L,1}$ of the CPL arrive at their equilibrium points $196.64V$ and $1.5256A$, respectively. As shown in Figure 2 (b), the state-norm term $\|\bar{x}(t)\|^2$ is being bounded by the exponential bound $\mathcal{B} = 1.9e5e^{-3t} + \mathcal{B}_\infty$ during the running process and finally bounded by the ultimate bound $\mathcal{B}_\infty = 0.1509$, which confirms the GEUB stability in mean square in Definition 1. For the disturbance rejection performance, due to $\varrho(\bar{x}(0)) > 0$, $\|z(t)\|_\infty = 0.78 \leq \zeta\|\omega(t)\|_\infty + \varrho(\bar{x}(0)) = 1.03 + \varrho(\bar{x}(0))$ holds, which guarantees the \mathcal{L}_∞ -gain in Definition 2.

As shown in Figure 1, the controller receives quantized data and generates control signals for injection current. Take the voltage $v_{C,1}$ in Figure 3 (a) for example, the DETM only releases some of the sampled data which satisfy the triggering condition, and all released data of the DETM are quantized into different levels. Figure 3 (b) shows the dynamics of the injection current. Due to the effect of the DETM, the injection current holds during each updating interval of the event-triggered controller, while FDI attacks randomly tamper the injection current.

As shown in Figure 4 (b), the DETM releases only 738 of the 2000 sampled data with a triggering rate $R_t = 36.9\%$, which implies the DETM consumes 63.1% less resources than the TTM. The minimum triggering interval is the sampling period $0.1ms$, and thus Zeno behavior is avoided. As shown in Figure 4 (a), FDI attacks randomly tamper 84 of the 738 released data of the DETM with an attacking rate 11.4%. Thus, although the DETM transmits only 36.9% of the sampling data and FDI attacks randomly tampered 11.4% of the triggered data, the designed ETFQIC controller still guarantees satisfactory system performance.

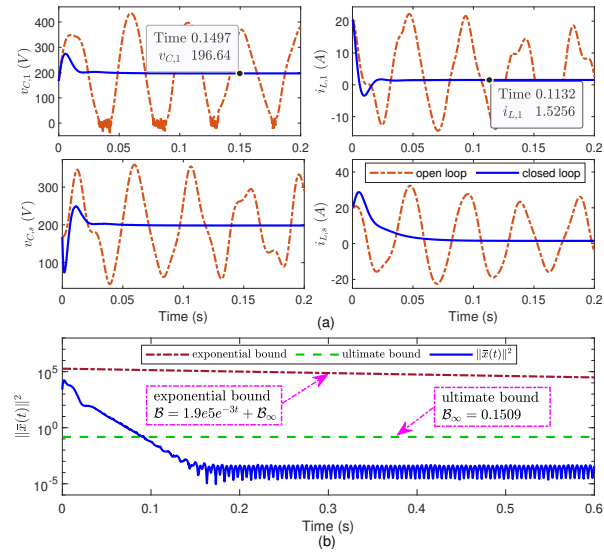


Figure 2. System responses of the DC microgrid.

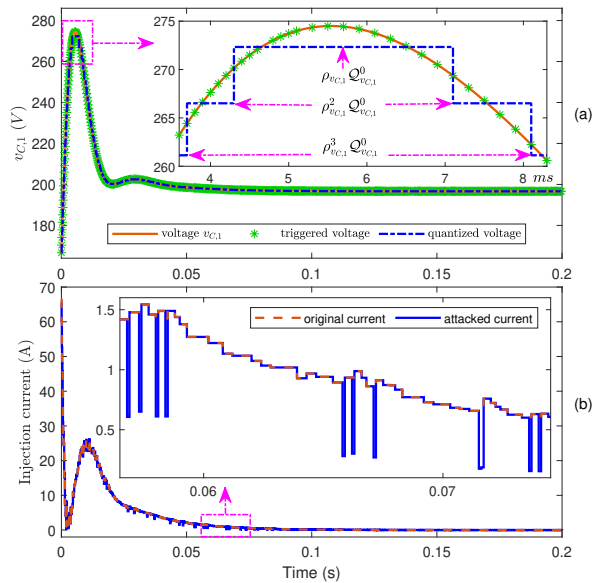


Figure 3. The quantized voltage and the injection current \bar{i}_c .

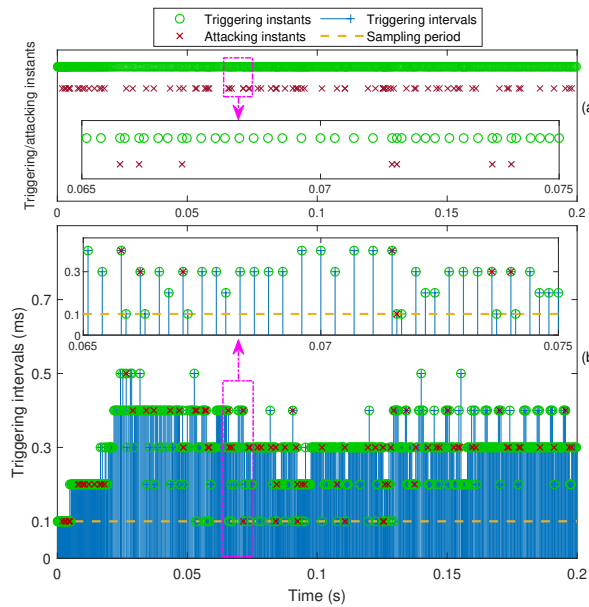


Figure 4. Characteristics of the dynamic ETM and the FDI attacks.

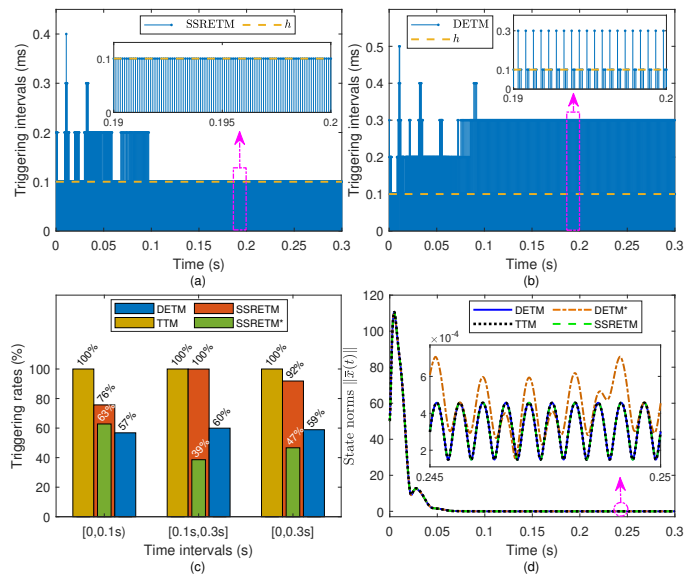


Figure 5. Comparison of the DETM and SSRETMs (Li et al., 2022; Liu et al., 2021; Zhang and Zhang, 2022).

Comparison with the SSRETM_s in (Li et al., 2022; Liu et al., 2021; Zhang and Zhang, 2022)

Considering the aforementioned microgrid with the PB disturbances $\omega(t) = 2\sin(2\pi 1e3t)$, the performances of the DETM (6) and SSRETM_s (Li et al., 2022; Liu et al., 2021; Zhang and Zhang, 2022) will be compared. During the steady-state period $[0.1s, 0.3s]$, the SSRETM_s ($\delta_s = 3e - 4$) in Figure 5 (a) almost reduce to the TTM. However, due to inclusion of the constant threshold δ_0 , the proposed DETM ($\delta_s, \delta_d = 3e - 4, \delta_0 = 2e - 5$) in Figure 5 (b) can still obtain large triggering intervals.

As shown in Figure 5 (c), during the transient period $[0, 0.1s]$, compared with the SSRETM_s' triggering rate 76%, the DETM's triggering rate 57% is lower, since the dynamic threshold term $\delta_d(t)$ of the DETM is large. During the steady period $[0.1s, 0.3s]$, compared with the SSRETM_s' triggering rate 100%, the DETM's triggering rate 60% is much lower, since the DETM contains a constant threshold δ_0 . Therefore, during the whole period $[0, 0.3s]$, the DETM' triggering rate 59% is lower than 92% of the SSRETM_s. Compared with the SSRETM* which marks the SSRETM working without disturbances, the SSRETM's performance deteriorates seriously under PB disturbances. Especially, during the steady-state period $[0.1s, 0.3s]$, the triggering rate of the SSRETM increases to 100%, i.e., it works as the TTM. These observations confirm Remark 2.

As shown in Figure 5 (d), compared with the SSRETM_s and TTM, the DETM obtains almost identical control performance, although its triggering rate is the lowest. The DETM* refers to the DETM with a larger constant threshold $\delta_0 = 1.2e - 3$. Compared with the DETM with a triggering rate 59%, the triggering rate 15% of the DETM* is lower. However, the control performance under the DETM* is worse than that under the DETM. Therefore, by adjust the parameter δ_0 of the DETM, tradeoffs can be made between control and communication performances, which confirms Remark 4.

Comparison with the method in (Herrera et al., 2017)

Using the aforementioned DC microgrid with quantizer, the method in (Herrera et al., 2017) and the proposed Theorem 2 design respectively the robust controller and fuzzy controller as

$$\begin{cases} \text{Robust controller:} \\ K = \begin{bmatrix} -0.1310 & 0.0146 & 0.8014 & 0.1055 \end{bmatrix} \\ \text{T-S fuzzy controller:} \\ K_1 = \begin{bmatrix} 1.2074 & 0.1162 & 0.0254 & 0.2597 \end{bmatrix} \\ K_2 = \begin{bmatrix} 1.1994 & 0.1200 & 0.0372 & 0.2604 \end{bmatrix} \end{cases}$$

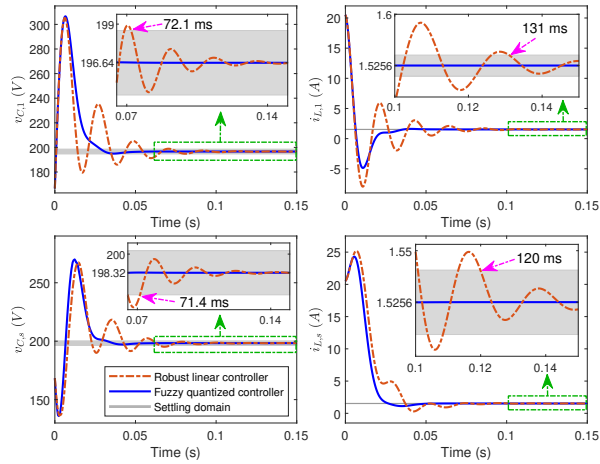


Figure 6. Performances of the robust controller (Herrera et al., 2017) and the proposed fuzzy controller.

Table 2. Settling times under different controllers

Methods	Settling times			
	$v_{C,1}$	$i_{L,1}$	$v_{C,s}$	$i_{L,s}$
Robust controller (Herrera et al., 2017)	72.1ms	131ms	71.4ms	120ms
Fuzzy controller	28.4ms	53.8ms	31.9ms	53.2ms

As shown in Figure 6, compared with the robust controller (Herrera et al., 2017), the proposed fuzzy controller achieves shorter settling times and lower overshoots. Table 2 presents the settling times under different controllers. Taking $v_{C,1}$ for instance, compared with the settling time 72.1ms of the robust controller (Herrera et al., 2017), the settling time of the proposed fuzzy controller drops to 28.4ms. These observations confirm Remark 1.

Conclusion

The paper has investigated the fuzzy \mathcal{L}_∞ control of DC microgrids with CPLs subject to the DETM, cyber attacks, quantizer, PB disturbances, premise mismatching and delays. First, by introducing a state-unrelated constant threshold, the proposed DETM is more robust to the PB disturbances than the SSRETMs, and its discrete-time feature naturally excludes Zeno behavior. Second, by virtually dividing the nonuniform triggering intervals of the DETM, a time-delayed fuzzy system model is build, which presents a unified platform to study effects of DETM, cyber attacks, quantizer, PB disturbances, premise mismatching and delays. Third, sufficient conditions for the GEUB stability in mean square

with guaranteed \mathcal{L}_∞ -gain are derived, and the relationship between the ultimate bound of the microgrid states and the constant threshold of the DETM is established. Further, a co-design method is provided to design simultaneously the DETM and the ETFQIC controller, which overcomes the inconvenience of the emulation method requiring two design steps. Simulation results confirm that, although only 36.9% of the periodic sampled data are released by the DETM, and cyber attacks tamper 11.4% of the DETM's released data, the proposed ETFQIC controller can still stabilize the DC microgrid system with guaranteed \mathcal{L}_∞ -gain. Compared with the SSRETMs, when considering the PB disturbances, the proposed DETM achieves lower triggering rate. Compared with the robust controller, the proposed fuzzy controller achieves smaller overshoot and shorter settling time.

Acknowledgements

The authors would like to thank the Editor, Associate Editor and Reviewers for their constructive comments and suggestions to improve the quality of the paper.

Disclosure statement

No potential conflict of interest was reported by the authors.

Funding

This work was supported by National Natural Science Foundation of China under Grant [number 61703146, 62173218]; Scientific and Technological Project of Henan Province under Grant [number 232102110268, 202102110126]; Backbone Teacher Project of Henan Province under Grant [number 2020GGJS048]. Henan Provincial Science and Technology Commissioner. International Corporation Project of Shanghai Science and Technology Commission under Grant [number 21190780300].

Data Availability Statement

Data sharing not applicable - no new data generated.

References

Aslam MS, Tiwari P, Pandey HM and Band SS (2023) Observer-based control for a new stochastic maximum power point tracking for photovoltaic systems with networked control system. *IEEE Transactions on Fuzzy Systems* 31(6): 1870 – 1884.

- Cecilia A, Sahoo S, Dragičević T, Costa-Castelló R and Blaabjerg F (2022) On addressing the security and stability issues due to false data injection attacks in DC microgrids—an adaptive observer approach. IEEE Transactions on Power Electronics 37(3): 2801–2814.
- Cespedes M, Xing L and Sun J (2011) Constant-power load system stabilization by passive damping. IEEE Transactions on Power Electronics 26(7): 1832–1836.
- Donkers MCF and Heemels WPMH (2012) Output-based event-triggered control with guaranteed \mathcal{L}_∞ -gain and improved and decentralized event-triggering. IEEE Transactions on Automatic Control 57(6): 1362 – 1376.
- Duan GR and Yu HH (2013) LMI in Control Systems Analysis, Design and Applications. Boca Raton, FL, USA: CRC Press.
- Fan S, Wu F and Liu H (2022) Unified closed-loop control and parameters design of buck-boost current-fed isolated DC-DC converter with constant power load. IEEE Journal of Emerging and Selected Topics in Power Electronics 10(4): 4207 – 4217.
- Habibi MR, Baghaee HR, Blaabjerg F and Dragičević T (2022) Secure MPC/ANN-based false data injection cyber-attack detection and mitigation in DC microgrids. IEEE Systems Journal 16(1): 1487–1498.
- Herrera L, Zhang W and Wang J (2017) Stability analysis and controller design of DC microgrids with constant power loads. IEEE Transactions on Smart Grid 8(2): 881 – 888.
- Hossain MM, Peng C, Sun HT and Xie S (2022) Bandwidth allocation-based distributed event-triggered LFC for smart grids under hybrid attacks. IEEE Transactions on Smart Grid 13(1): 820–830.
- Hu S, Yue D, Dou C, Xie X, Ma Y and Ding L (2022) Attack-resilient event-triggered fuzzy interval type-2 filter design for networked nonlinear systems under sporadic denial-of-service jamming attacks. IEEE Transactions on Fuzzy Systems 30(1): 190–204.
- Jiao YT, Ding L, Kong ZM and Chen CY (2023) Distributed observer-based resilient control of islanded DC microgrids under actuator faults. Transactions of the Institute of Measurement and Control 45: 1 – 17.
- Kang W, Chen M, Guan Y, Tang L, Vasquez Q JC and Guerrero JM (2022) Distributed event-triggered optimal control method for heterogeneous energy storage systems in smart grid. IEEE Transactions on Sustainable Energy 13(4): 1944–1956.
- Li F, Li K, Peng C and Gao L (2023a) Dynamic event-triggered fuzzy control of DC microgrids under FDI attacks and imperfect premise matching. International Journal of Electrical Power and Energy Systems 147: 1–12.
- Li F, Li K, Peng C and Gao L (2023b) Dynamic event-triggered fuzzy non-fragile control of DC microgrids. ISA Transactions 142: 83 – 97.
- Li Z, Cheng Z, Si J and Li S (2022) Distributed event-triggered hierarchical control to improve economic operation of hybrid AC/DC microgrids. IEEE Transactions on Power Systems 37(5): 3653 – 3668.
- Liu J, Wang Y, Zha L, Xie X and Tian E (2021) An event-triggered approach to security control for networked systems using hybrid attack model. International Journal of Robust and Nonlinear Control 31(12): 5796 – 5812.

- Mardani MM, Vafamand N, Khooban MH, Dragičević T and Blaabjerg F (2019) Design of quadratic D-stable fuzzy controller for DC microgrids with multiple CPLs. IEEE Transactions on Industrial Electronics 66(6): 4805–4812.
- Naami G, Ouahi M, Sadek BA, Tadeo F and Rabhi A (2022) Delay-dependent h_∞ dynamic observers for non-linear systems with multiple time-varying delays. Transactions of the Institute of Measurement and Control 44(15): 2998 – 3015.
- Peng C and Han QL (2013) A novel event-triggered transmission scheme and \mathcal{L}_2 control co-design for sampled-data control systems. IEEE Transactions on Automatic Control 58(10): 2620 – 2626.
- Peng C and Li F (2018) A survey on recent advances in event-triggered communication and control. Information Sciences 457-458: 113 – 125.
- Peng C, Ma S and Xie X (2017) Observer-based non-PDC control for networked T–S fuzzy systems with an event-triggered communication. IEEE Transactions on Cybernetics 47(8): 2279–2287.
- Peng C and Yang TC (2013) Event-triggered communication and H_∞ control co-design for networked control systems. Automatica 49(5): 1326 – 1332.
- Peng J, Fan B, Yang Q and Liu W (2021) Distributed event-triggered control of DC microgrids. IEEE Systems Journal 15(2): 2504–2514.
- Prasad S (2023) Robust sliding mode controller for frequency regulation in a microgrid. Transactions of the Institute of Measurement and Control 45(10): 1947 – 1964.
- Samanta S, Barman S, Mishra JP, Roy P and Roy BK (2021) Energy management and damping improvement of a DC microgrid with constant power load using interconnection and damping assignment-passivity based control. Transactions of the Institute of Measurement and Control 43(7): 1545 – 1559.
- Shafiee P, Khayat Y, Batmani Y, Shafiee Q and Guerrero JM (2021) On the design of event-triggered consensus-based secondary control of DC microgrids. IEEE Transactions on Power Systems : 1–12.
- Shi M, Shahidehpour M, Zhou Q, Chen X and Wen J (2021) Optimal consensus-based event-triggered control strategy for resilient DC microgrids. IEEE Transactions on Power Systems 36(3): 1807 – 1818.
- Vafamand N, Khooban MH, Dragičević T and Blaabjerg F (2019) Networked fuzzy predictive control of power buffers for dynamic stabilization of DC microgrids. IEEE Transactions on Industrial Electronics 66(2): 1356–1362.
- Wang W, Postoyan R, Nesic D and Heemels W (2020) Periodic event-triggered control for nonlinear networked control systems. IEEE Transactions on Automatic Control 65(2): 620 – 635.
- Xie Z and Wu Z (2023) Distributed fault-tolerant secondary control for DC microgrids against false data injection attacks. International Journal of Electrical Power and Energy Systems 144: 108599.
- Xing JW, Peng C, Cao Z and Xie WB (2023) Security-based control for networked interval type-2 fuzzy systems with multiple cyber-attacks: an improved dynamic event-triggered scheme. IEEE Transactions on Fuzzy Systems

31(8): 2747–2760.

Xing L, Xu Q, Guo F, Wu ZG and Liu M (2021) Distributed secondary control for DC microgrid with event-triggered signal transmissions. IEEE Transactions on Sustainable Energy 12(3): 1801–1810.

Xu Q, Vafamand N, Chen L, Dragičević T, Xie L and Blaabjerg F (2021) Review on advanced control technologies for bidirectional DC/DC converters in DC microgrids. IEEE Journal of Emerging and Selected Topics in Power Electronics 9(2): 1205–1221.

Zhang J, Peng C and Xie X (2023) Platooning control of vehicular systems by using sampled positions. IEEE Transactions on Circuits and Systems II: Express Briefs 70(7): 2435–2439.

Zhang J and Zhang H (2022) A high-reliability event-triggered secondary control strategy for microgrid considering time-varying delay. IEEE Systems Journal : 1–12.

Zhang L, Liang H, Sun Y and Ahn CK (2021) Adaptive event-triggered fault detection scheme for semi-markovian jump systems with output quantization. IEEE Transactions on Systems, Man, and Cybernetics: Systems 51(4): 2370 – 2381.

Zhou J, Yang Q, Chen X, Chen Y and Wen J (2023) Resilient distributed control against destabilization attacks in DC microgrids. IEEE Transactions on Power Systems 38(1): 371 – 384.

Zou L, Wang Z, Han QL and Zhou D (2017) Ultimate boundedness control for networked systems with try-once-discard protocol and uniform quantization effects. IEEE Transactions on Automatic Control 62(12): 6582–6588.